Light diffusion in *N*-layered turbid media: steady-state domain

André Liemert
Alwin Kienle
Institut für Lasertechnologien in der Medizin und
    Meßtechnik
Helmholtzstrasse 12
Ulm, D-89081 Germany

Abstract. We deal with light diffusion in *N*-layered turbid media. The steady-state diffusion equation is solved for *N*-layered turbid media having a finite or an infinitely thick *N*'th layer. Different refractive indices are considered in the layers. The Fourier transform formalism is applied to derive analytical solutions of the fluence rate in Fourier space. The inverse Fourier transform is calculated using four different methods to test their performance and accuracy. Further, to avoid numerical errors, approximate formulas in Fourier space are derived. Fast solutions for calculation of the spatially resolved reflectance and transmittance from the *N*-layered turbid media (≈ 10 ms) with small relative differences ($< 10^{-7}$) are found. Additionally, the solutions of the diffusion equation are compared to Monte Carlo simulations for turbid media having up to 20 layers. © *2010 Society of Photo-Optical Instrumentation Engineers.* [DOI: 10.1117/1.3368685]

1 Introduction

Many different parts of the human body exhibit a layered structure, e.g., the head or the extremities. To calculate the light propagation in these layered tissues, which is important for the application of light in therapeutical and diagnostic medicine, fast and accurate forward solutions are required.

Usually, it is assumed that the radiative transfer theory correctly describes light propagation in biological media.[1,2] Most often, the Monte Carlo method is used to solve the radiative transfer equation numerically. To obtain faster solutions describing the light propagation in biological tissue, the diffusion equation, which is an approximation to the radiative transfer theory, is applied.[1]

Several solutions of the layered diffusion equation have been reported in literature. Dayan et al. applied a Fourier formalism to solve the two-layered diffusion equation. However, to be able to obtain analytical solutions several approximations were introduced in the inverse Fourier calculations.[3] We derived exact solutions for the two-layered geometry in the steady-state, frequency, and time domains[4–6] by numerically performing the inverse Fourier transform and introducing appropriate boundary conditions. Subsequently, different groups have used these solutions for further investigations.[7,8] Additionally, the solutions have been extended, for example, to a hybrid Monte Carlo/diffusion scheme,[9] to a tilted interface between the layers,[10] or to diffusing wave spectroscopy.[11]

Supplementally, different approaches to solve the layered diffusion equation have been made. Tualle et al. applied the method of images to derive solutions of the two-layered geometry,[12] whereas Martelli et al. used the eigenfunction method together with the separation of variables technique to solve the time-dependent diffusion equation for two and three layers.[13–15] Barnett solved the *N*-layered diffusion equation via a finite-difference method.[16] Recently, an approach based on the solution of a single layer to obtain the solutions for many layers using convolution was proposed.[17]

Building on our earlier work we solved the diffusion equation for *N*-layered turbid media in the steady-state, frequency, and time domains and compared the results with Monte Carlo simulations. The solutions were derived for a semi-infinite layered and for a finite layered geometry, i.e., the bottom layer has an infinite and finite thickness, respectively. Recently, independently of us, solutions of the *N*-layered diffusion equation have been published based on our earlier work for the special case of semi-infinite turbid media.[18,19] Whereas the extension of the Fourier formalism to *N* layers is straightforward, the decisive point is the numerically correct and efficient 2-D inverse Fourier transform. To this end, we implemented four different methods to obtain the solutions in real space. Additionally, approximate solutions for the fluence rate in Fourier space were derived to avoid numerical errors due to the inverse Fourier transform.

In this paper, the light diffusion in turbid media is considered in the steady-state domain, whereas in the accompanying paper[20] the light diffusion in the frequency and time domains is analyzed. Turbid media consisting of up to 20 layers having matched and mismatched refractive indices are studied, showing good agreement between the solutions of the diffusion theory and Monte Carlo simulations. The four methods for calculating the inverse Fourier transform are analyzed to op-

Address all correspondence to: André Liemert, Institut für Lasertechnologien in der Medizin und Meßtechnik, Helmholtzstrasse 12, Ulm, D-89081 Germany. Tel: 49-731-1429 24; E-mail: andre.liemert@ilm.uni-ulm.de
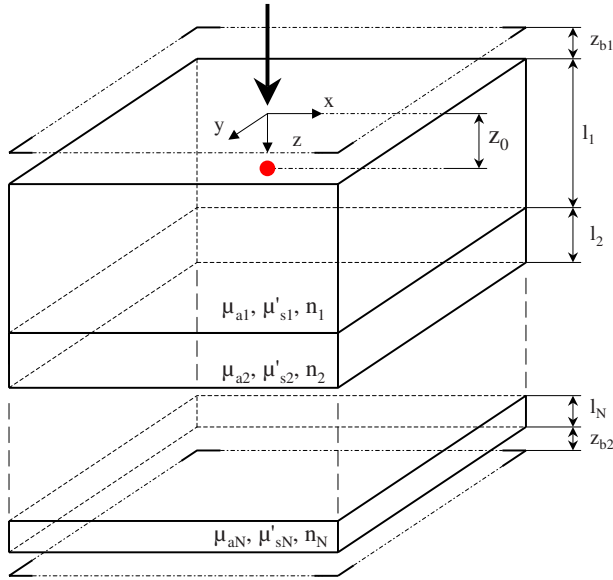
Fig. 1 Scheme of the *N*-layered turbid medium including the position of the source and the extrapolated boundaries.

timize the performance of the solutions. Explicit solutions are given in the appendix for turbid media having two, three, and four layers for both the semi-infinite and the finite bottom layer. In addition, an executable program for calculation of the reflectance from an *N*-layered turbid medium is provided on the Internet.[21]

2 Theory

In this section, the steady-state diffusion equation for an *N*-layered turbid medium having laterally infinite extensions is derived using the Fourier transform formalism. A pencil light beam is incident in the *z* direction perpendicular to the interface between the first layer and the nonscattering surrounding (see Fig. 1).

The origin of the coordinate system is the point of light impact on the turbid medium. As in our earlier paper, it is assumed that the light beam can be characterized by an isotropic point source at a depth $z = z_0 = 1/(\mu_{a1} + \mu'_{s1})$ in the first layer, $\delta(x, y, z - z_0)$, where μ_{a1} and μ'_{s1} are the absorption and reduced scattering coefficients of the first layer, respectively.[4] For this geometry, the diffusion equation becomes

$$D_1 \Delta \Phi_1(x, y, z) - \mu_{a1} \Phi_1(x, y, z) = -\delta(x, y, z - z_0), \quad 0 \leq z < l_1, \tag{1}$$

$$D_k \Delta \Phi_k(x, y, z) - \mu_{ak} \Phi_k(x, y, z) = 0, \quad \sum_{j=1}^{k-1} l_j < z \leq \sum_{j=1}^{k} l_j,$$
$$k = 2, 3, \ldots, N, \tag{2}$$

where l_k is the thickness of layer k, Φ_k is the fluence rate, $D_k = 1/[3(\mu'_{sk} + \mu_{ak})]$ is the diffusion coefficient, and μ'_{sk} and μ_{ak} are the reduced scattering and absorption coefficients of layer k, respectively.

We solved this system of equations using the Fourier transform approach and extrapolated boundary conditions. First, the equations are two-dimensionally Fourier transformed from the real space into the Fourier space with respect to the *x* and *y* coordinates. The boundary conditions depending only on the *z* coordinate are applied in the Fourier space. The resulting system of equations is solved, yielding the solutions in the Fourier space. Finally, these solutions are two-dimensionally inverse Fourier transformed, delivering the solutions in the real space.

We start by applying the 2-D Fourier transform:

$$\Phi_k(z, s_1, s_2) = \int_{-\infty}^{\infty} \int_{-\infty}^{\infty} \Phi_k(x, y, z) \exp[i(s_1 x + s_2 y)] dx dy, \tag{3}$$

to Eqs. (1) and (2), and obtain

$$\frac{\partial^2}{\partial z^2} \Phi_1(z, s) - \alpha_1^2 \Phi_1(z, s) = -\frac{1}{D_1} \delta(z - z_0), \quad 0 \leq z < l_1, \tag{4}$$

$$\frac{\partial^2}{\partial z^2} \Phi_k(z, s) - \alpha_k^2 \Phi_k(z, s) = 0, \quad \sum_{j=1}^{k-1} l_j < z \leq \sum_{j=1}^{k} l_j,$$
$$k = 2, 3, \ldots, N, \tag{5}$$

with $s = (s_1^2 + s_2^2)^{1/2}$ and $\alpha_k^2 = (D_k s^2 + \mu_{ak})/D_k$. The fluence rate in the Fourier space in layer k is denoted by $\Phi_k(z, s)$. The following boundary conditions are used in the Fourier space for an *N*-layered turbid medium having a finite thick *N*'th layer:

$$\Phi_1(-z_{b_1}, s) = 0, \tag{6}$$

$$\Phi'_1(z_0, s) = \Phi_1(z_0, s), \tag{7}$$

$$\left. \frac{\partial \Phi_1(z, s)}{\partial z} \right|_{z=z_0} - \left. \frac{\partial \Phi'_1(z, s)}{\partial z} \right|_{z=z_0} = \frac{1}{D_1}, \tag{8}$$

$$\frac{\Phi_k(L_k, s)}{\Phi_{k+1}(L_k, s)} = \left(\frac{n_k}{n_{k+1}} \right)^2, \quad L_k = \sum_{j=1}^{k} l_j, \quad 1 \leq k \leq N-1, \tag{9}$$

$$D_k \left. \frac{\partial \Phi_k(z, s)}{\partial z} \right|_{z=L_k} = D_{k+1} \left. \frac{\partial \Phi_{k+1}(z, s)}{\partial z} \right|_{z=L_k}, \quad L_k = \sum_{j=1}^{k} l_j,$$
$$1 \leq k \leq N-1, \tag{10}$$

$$\Phi_N(L_N + z_{b_2}, s) = 0, \tag{11}$$

where $\Phi_1(z, s)$ and $\Phi'_1(z, s)$ are the fluence rate in the first layer in the Fourier space above the δ source and below the delta source, respectively. The refractive index of layer k is denoted by n_k, and L_k is the total thickness of the turbid medium. Equations (7) and (8) describe the fluence rate and its

derivative at the position of the δ source, and Eqs. (9) and (10) at the interfaces of the different turbid layers. In Eqs. (6) and (11), z_{b_1} and z_{b_2} are the positions of the extrapolated boundaries above the first and below the *N*'th layer, respectively (see Fig. 1), where the fluence rate is set to zero.[22] These quantities are obtained using

$$z_{b1} = \frac{1 + R_{\text{eff},1}}{1 - R_{\text{eff},1}} 2D_1, \quad z_{b2} = \frac{1 + R_{\text{eff},N}}{1 - R_{\text{eff},N}} 2D_N, \qquad (12)$$

where $R_{\text{eff},k}$ represents the fraction of photons that is internally diffusely reflected at the boundary to the nonscattering

surrounding at the top or at the bottom layer. We calculated $R_{\text{eff},k}$ by solving the integrals derived by Haskell et al.[22]

In the case of an *N*-layered turbid medium having an infinitely thick *N*'th layer, Eq. (11) becomes

$$\Phi_N(\infty, s) = 0. \qquad (13)$$

We solved the resulting equation system for *N* layers having a finite and semi-infinitely thick *N*'th layer by applying Cramer's rule. The general solution for *N* layers was obtained by induction using the solutions for two, three, and four layers. In the first case, we obtain for the fluence rate in the first layer (above the delta source)

$$\Phi_1(z,s) = \frac{\sinh[\alpha_1(z_0 + z_{b_1})]}{\alpha_1 D_1} \frac{\alpha_1 \beta_3 D_1 \cosh[\alpha_1(l_1 - z)] + \alpha_2 \gamma_3 D_2(n_2^2/n_1^2)\sinh[\alpha_1(l_1 - z)]}{N(z,s)} - \frac{\sinh[\alpha_1(z_0 - z)]}{\alpha_1 D_1}, \qquad (14)$$

and for the fluence rate in the *N*'th layer

$$\Phi_N(z,s) = \frac{\prod\limits_{k=2}^{N-1} \alpha_k D_k (n_N/n_1)^2 \sinh[\alpha_1(z_0 + z_{b1})]\sinh[\alpha_N(L_N + z_{b2} - z)]}{N(z,s)}, \qquad (15)$$

where $N(z,s)$ is

$$N(z,s) = \alpha_1 \beta_3 D_1 \cosh[\alpha_1(l_1 + z_{b_1})] + \alpha_2 \gamma_3 D_2\left(\frac{n_2^2}{n_1^2}\right)\sinh[\alpha_1(l_1 + z_{b_1})]. \qquad (16)$$

The quantities β_3 and γ_3 in Eqs. (14) and (16) are obtained by using recursion formulas. By applying β_N and γ_N,

$$\begin{pmatrix} \beta_N \\ \gamma_N \end{pmatrix} = \alpha_{N-1} D_{N-1} \sinh[\alpha_N(l_N + z_{b2})]\begin{bmatrix} \cosh(\alpha_{N-1}l_{N-1}) \\ \sinh(\alpha_{N-1}l_{N-1}) \end{bmatrix} + \alpha_N D_N\left(\frac{n_N^2}{n_{N-1}^2}\right)\cosh[\alpha_N(l_N + z_{b2})]\begin{bmatrix} \sinh(\alpha_{N-1}l_{N-1}) \\ \cosh(\alpha_{N-1}l_{N-1}) \end{bmatrix}, \qquad (17)$$

as start terms the quantities β_3 and γ_3 are obtained for an *N*-layered turbid medium by iteratively using

$$\begin{pmatrix} \beta_{k-1} \\ \gamma_{k-1} \end{pmatrix} = \begin{bmatrix} \alpha_{k-2}D_{k-2}\cosh(\alpha_{k-2}l_{k-2}) & \alpha_{k-1}D_{k-1}\left(\dfrac{n_{k-1}^2}{n_{k-2}^2}\right)\sinh(\alpha_{k-2}l_{k-2}) \\[2mm] \alpha_{k-2}D_{k-2}\sinh(\alpha_{k-2}l_{k-2}) & \alpha_{k-1}D_{k-1}\left(\dfrac{n_{k-1}^2}{n_{k-2}^2}\right)\cosh(\alpha_{k-2}l_{k-2}) \end{bmatrix}\begin{pmatrix} \beta_k \\ \gamma_k \end{pmatrix}, \qquad (18)$$

for $k=N, N-1, \ldots, 4$, i.e., until β_3 and γ_3 are obtained. This means that for $N=3$, Eq. (17) can be directly applied without using Eq. (18). We give the fluence rate of the first and *N*'th layers, because we are interested in the reflectance from the first and the transmittance from the *N*'th layer, which are calculated from the fluence rates of these layers.

In the second case, the semi-infinite *N*-layered turbid medium $(L_N \rightarrow \infty)$, the fluence rate $\Phi_1(z,s)$ is again calculated with Eq. (14), but the start terms for computing β_3 and γ_3 are now

$$\begin{pmatrix} \beta_N \\ \gamma_N \end{pmatrix} = \alpha_{N-1}D_{N-1}\begin{bmatrix} \cosh(\alpha_{N-1}l_{N-1}) \\ \sinh(\alpha_{N-1}l_{N-1}) \end{bmatrix} + \alpha_N D_N\left(\frac{n_N^2}{n_{N-1}^2}\right)$$
$$\times \begin{bmatrix} \sinh(\alpha_{N-1}l_{N-1}) \\ \cosh(\alpha_{N-1}l_{N-1}) \end{bmatrix}. \qquad (19)$$

The recursion formula is the same as for the finite *N*-layered turbid medium, see Eq. (18). For the semi-infinite *N*-layered turbid medium we give only the fluence rate in the first layer, because the transmittance is zero. With these equations, the analytical formula of the fluence rate in the Fourier space is obtained for *N*-layered turbid media for $N \geqslant 3$. In the appendix, we also give the solutions for two-layered turbid media for the finite and infinite cases. In addition, the explicit

formulas for three and four layers are also presented for the finite and infinite thick bottom layer.

Next, the 2-D inverse Fourier transform of $\Phi(z,s)$ must be calculated to obtain the fluence rate in real space $\Phi(x,y,z)$. We performed these transforms numerically as no general analytical solution was found up to now. For the accuracy of the calculation of the fluence rate in real space, this step is decisive. To minimize the numerical errors, we first used approximate solutions for large s values (see Sec. 5.2). Second, we programmed and compared four different methods to accomplish the 2-D inverse Fourier transform:

$$\Phi_k(x,y,z) = \frac{1}{(2\pi)^2} \int_{-\infty}^{\infty} \int_{-\infty}^{\infty} \Phi_k(z,s) \exp[-i(s_1 x + s_2 y)] \mathrm{d}s_1 \, \mathrm{d}s_2.$$

(20)

In method A, Eq. (20) was solved numerically by evaluating it at discrete s_1 and s_2 values using a DFT (discrete Fourier transform). The FFT (fast Fourier transform) algorithm was applied to accelerate the calculations.[23] Due to the rotational symmetry, it is sufficient to calculate the fluence rate in one direction.

In method B, we expressed $\Phi_k(x,y,z)$ in a 2-D Fourier series:

$$\Phi_k(x,y,z) = \frac{\Delta s_1 \Delta s_2}{(2\pi)^2} \sum_{m=-\infty}^{\infty} \sum_{n=-\infty}^{\infty} \Phi_k(m\Delta s_1, n\Delta s_2)$$
$$\times \exp[-i(m\Delta s_1 x + n\Delta s_2 y)].$$

(21)

By accurate sampling of Φ_k in the Fourier space and by regarding only the central solution of the resulting periodic function, $\Phi_k(x,y,z)$ is obtained without significant aliasing. Equation (21) can be simplified by using the rotational symmetry of the considered geometry:

$$\Phi_k(x,y,z) = \frac{\Delta s_1 \Delta s_2}{(2\pi)^2} \sum_{m=-\infty}^{\infty} \sum_{n=-\infty}^{\infty} \Phi_k(m\Delta s_1, n\Delta s_2)$$
$$\times \cos(m\Delta s_1 x)\cos(n\Delta s_2 y).$$

(22)

Again, it is sufficient to evaluate Φ_k in one direction (e.g., $y=0$). By simplifying the evaluation of the sums and assuming the same sampling rate in both directions ($\Delta s_1 = \Delta s_2 = \Delta s$) we finally get

$$\Phi_k(x,0,z) = \left(\frac{\Delta s}{2\pi}\right)^2 \Bigg\{ \Phi_k(0,0) + 2\sum_{m=1}^{\infty} \Phi_k(m\Delta s,0)$$
$$+ \Phi_k(m\Delta s,0)\cos(m\Delta s x)$$
$$+ 2\Phi_k(m\Delta s,m\Delta s)\cos(m\Delta s x)$$
$$+ 4\sum_{m=1}^{\infty}\sum_{n=m+1}^{\infty} \Phi_k(m\Delta s,n\Delta s)[\cos(m\Delta s x)$$
$$+ \cos(n\Delta s x)] \Bigg\}.$$

(23)

To obtain similar accuracy as for the other methods, we typically used 400 terms in the sums and a sampling rate in the range of $\Delta s \approx 20\mu_s'/400$. Note that the implementation of method B is the easiest of the four methods.

In the other two methods the rotational symmetry is used to obtain from Eq. (20) the 1-D inverse Hankel transform:

$$\Phi_k(\rho,z) = \frac{1}{2\pi} \int_0^{\infty} \Phi_k(z,s) s J_0(s\rho) \mathrm{d}s,$$

(24)

where J_0 denotes the Bessel function of first kind and zero order.

In method C, the integral is solved numerically by applying Gauss integration using typically 2 times 480 points.[23] For the upper limit of the integral, we used values in the range of $30 \times \mu_s'$. In our original paper concerning the solution of the two-layered turbid medium, this method was used to calculate the inverse Fourier transform.[4]

In method D, Eq. (24) is transformed into a correlation integral, which is then represented by a discrete correlation.[24] This can be evaluated efficiently with an FFT algorithm, which delivers the fluence rate at many (e.g., 512) distances. However, the distances are exponentially distributed. Alternatively, the discrete correlation can be evaluated at one distance without using the FFT algorithm.

By applying one or several of the four methods, the fluence rate $\Phi_1(\rho,z)$ is obtained. Then, the spatially resolved reflectance $R(\rho)$ from the first layer is computed using

$$R(\rho) = \int_{2\pi} \mathrm{d}\Omega [1 - R_f(\theta)] \frac{1}{4\pi} \Bigg[\Phi_1(\rho, z=0)$$
$$+ 3D_1 \left. \frac{\partial \Phi_1(\rho,z)}{\partial z} \right|_{z=0} \cos(\theta) \Bigg] \cos(\theta),$$

(25)

where $R_f(\theta)$ is the Fresnel reflection coefficient for a photon having an incident angle θ relative to the normal to the boundary. The use of the combined fluence rate and flux term in Eq. (25) is important to match better Monte Carlo simulations that use the Henyey-Greenstein function as a phase function with anisotropy factors typically found for biological media[25] ($0.7 < g < 1$). For the finite, thick *N*-layered tissue the transmittance is calculated with

$$T(\rho) = -D_N \left. \frac{\partial \Phi_N(\rho,z)}{\partial z} \right|_{z=L_N}.$$

(26)

To determine the transmittance, it is sufficient to use only the flux term to approximate the Monte Carlo simulations.

The solutions of the diffusion equations are compared with Monte Carlo simulations. The Monte Carlo method has been described in detail in the literature.[26] The salient features of our code are as follows. A pencil beam is incident in z direction perpendicular onto the turbid medium at the origin of the coordinate system. The Henyey-Greenstein function with an anisotropy factor of $g=0.8$ is applied as phase function. At the boundaries, the Fresnel reflection and transmission coefficients are used to consider the different refractive indices. Both the Monte Carlo simulations and the solutions of the
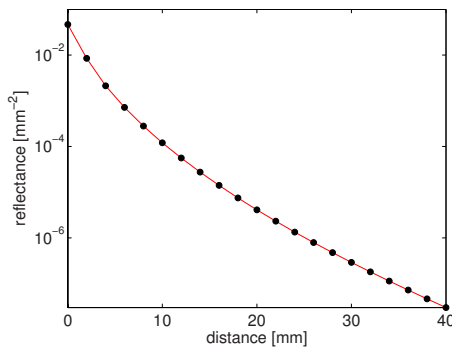
Fig. 2 Comparison of the reflectance from a semi-infinite two-layered turbid medium calculated with method C (solid curve) and method D (circles). The parameters are $\mu'_{s1}=1.0$ mm^{-1}, $\mu_{a1}=0.02$ mm^{-1}, $\mu'_{s2}=1.5$ mm^{-1}, $\mu_{a2}=0.005$ mm^{-1}, $l_1=5$ mm, $l_2=\infty$ mm, and $n_1=n_2=1.4$.

diffusion equations were programmed in Delphi (Pascal). Extended variables (19 to 20 significant digits; 10 bytes) are used to minimize numerical errors.

3 Results

In this section, we first show the results for the solutions of the diffusion equation obtained with the different methods for computing the inverse Fourier transform. Second, the solutions of the diffusion equations are compared to Monte Carlo simulations.

3.1 *Comparison of Different Methods for Calculation of the Inverse Fourier Transform*

The spatially resolved reflectance from *N*-layered turbid media was calculated using the four methods for computing the inverse Fourier transform, which are explained in the theory section. In general, we found that all four methods agreed excellently. Of course, the accuracy depends on the numerical efforts that have been applied. We chose the number of points used in the series or integral evaluations in the four methods such that the accuracy for calculation of $\Phi(\rho,z)$ was similar. As an example, we show the spatially resolved reflectance from a two-layered turbid medium calculated with method C (solid curve) and method D (circles) in Fig. 2.

No differences can be seen in the figure between the results obtained from the two methods. To distinguish both curves we calculated the relative difference between them, which is shown in Fig. 3.

The differences are $<10^{-7}$ for distances $\lesssim40$ mm from the incident source. These are typical differences that we found by comparing all four methods. In most cases, the differences are smaller for small distances compared to large distances from the incident source. Note that a high accuracy for the calculation of $\Phi(\rho,z)$ is especially necessary for reconstruction problems, i.e., the determination of the optical coefficients with, e.g., nonlinear regression routines.

As the numerical accuracy of the four models is similar, it is interesting to compare their execution times. For a layered turbid medium having typical optical properties found in biological media we got following typical calculation times for the reflectance or transmittance in real space using a state-of-
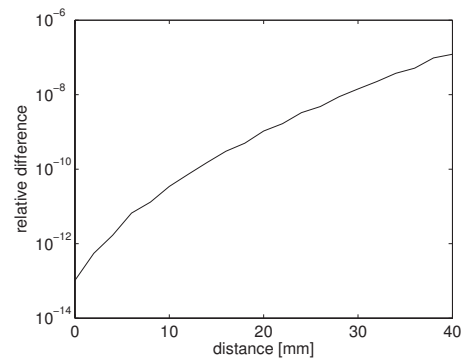

Fig. 3 Relative difference of the curves shown in Fig. 2 [(|method C − method D|)/method C].

the-art computer. With methods A, B, C, and D computation times of ≈3 s (for ≈1000 distances; by using the FFT one obtains many distances in one calculation), ≈100 ms (for one distance), ≈35 ms (for one distance), and ≈10 ms (for one distance) were needed, respectively. When the FFT was used to evaluate the correlation in method D (see Sec. 2) even ≈1000 distances could be evaluated in ≈10 ms. The disadvantage of using the FFT in methods A and D is that the fluence rate cannot be obtained for arbitrarily chosen distances. In method A, the distances are equidistant, and in method C, exponentially distributed.

3.2 *Comparison of the Solutions of the Diffusion Equation with Monte Carlo Simulations*

Figure 4 shows the influence of different refractive indices of the first layer on the spatially resolved reflectance. A two-layered semi-infinite turbid medium was considered having (1) a refractive index of 1.4 for both layers [green (lighter) curve and circles] and (2) a refractive index of 1.8 for the first and 1.4 for the second layer (black curve and circles). For the nonscattering surrounding, a refractive index of 1.0 was as-
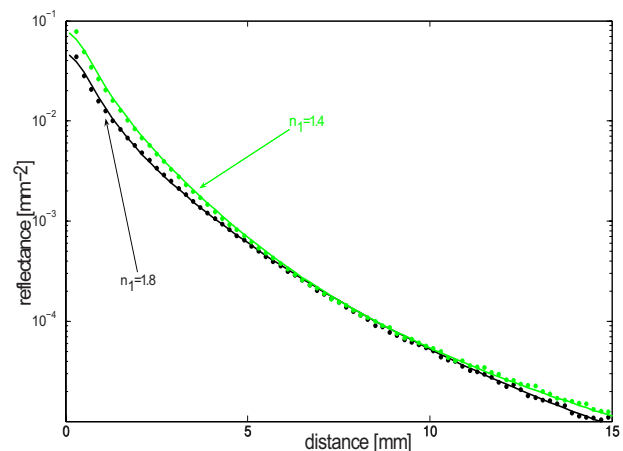

Fig. 4 Comparison of the solution of the semi-infinite two-layered diffusion equation and Monte Carlo simulations. The parameters are $\mu'_{s1}=1.3$ mm^{-1}, $\mu_{a1}=0.04$ mm^{-1}, $\mu'_{s2}=0.8$ mm^{-1}, $\mu_{a2}=0.005$ mm^{-1}, $l_1=3$ mm, and $l_2=\infty$ mm.
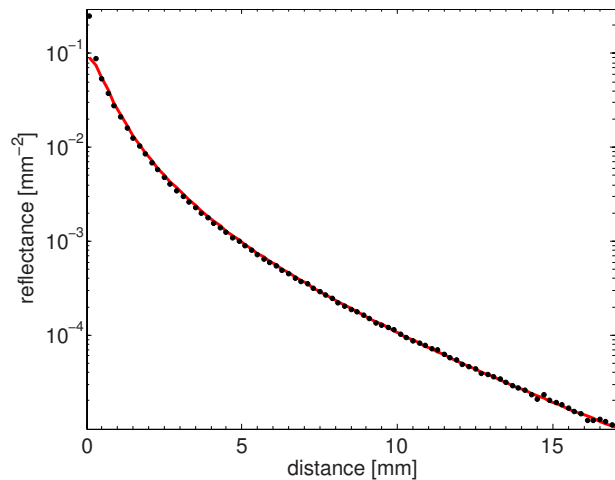
Fig. 5 Comparison of the solution of a 20-layered turbid medium calculated with the diffusion equation (solid curve) with Monte Carlo simulations (circles). Optical coefficients were randomly chosen but were the same for both methods. The refractive index of all layers was 1.4.

sumed. A good agreement between the Monte Carlo simulations (circles) and diffusion theory (solid curves) can be observed.

Figure 5 shows a comparison of diffusion theory and Monte Carlo simulations for reflectance from a turbid medium having 20 layers. The optical properties of the layers were randomly chosen in the range between $0.5 \text{ mm}^{-1} < \mu_s'$ $< 1.5 \text{ mm}^{-1}$ and $0.0 \text{ mm}^{-1} < \mu_a < 0.04 \text{ mm}^{-1}$, but were the same for the solution of the diffusion equation and Monte Carlo simulation. The thickness of each layer was 1 mm. Thus, the thickness of the whole turbid medium was 20 mm. The refractive index of each layer was 1.4, that of the non-scattering surrounding media was 1.0. Again, a good agreement between the two solutions can be stated except for small distances where the diffusion approximation is not valid.

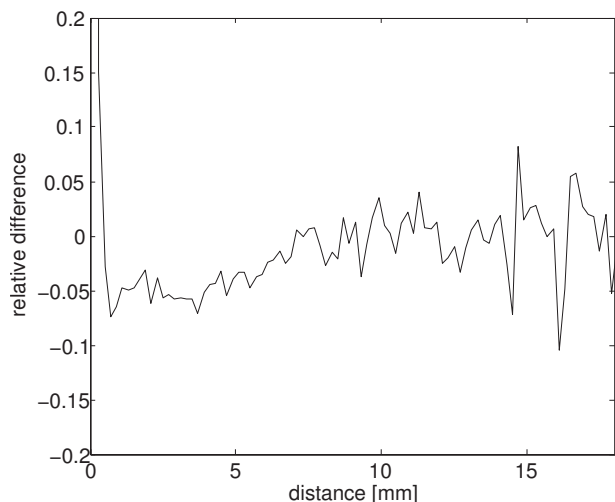Figure 6 gives the relative difference of both curves to

Fig. 6 Relative difference of the curves shown in Fig. 5 [(Monte Carlo−diffusion)/Monte Carlo].
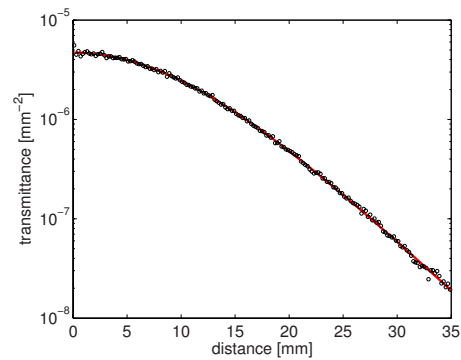

Fig. 7 Comparison of the solution of the semi-infinite four-layered diffusion equation (solid curve) with Monte Carlo simulations (circles). The parameters are $\mu_{s1}' = 1.6 \text{ mm}^{-1}$, $\mu_{a1} = 0.005 \text{ mm}^{-1}$, $\mu_{s2}' = 0.9 \text{ mm}^{-1}$, $\mu_{a2} = 0.015 \text{ mm}^{-1}$, $\mu_{s3}' = 0.7 \text{ mm}^{-1}$, $\mu_{a3} = 0.01 \text{ mm}^{-1}$, $\mu_{s4}' = 1.2 \text{ mm}^{-1}$, $\mu_{a4} = 0.02 \text{ mm}^{-1}$, $n_1 = 1.4$, $n_2 = 1.3$, $n_3 = 1.5$, $n_4 = 1.4$, $l_1 = 4 \text{ mm}$, $l_2 = 5 \text{ mm}$, $l_3 = 3 \text{ mm}$, and $l_4 = 12 \text{ mm}$.

better visualize the performance of the diffusion solution compared to the Monte Carlo simulation.

At small distances ($\rho < 1 \text{ mm}$) the differences are large, for intermediate distances the differences are about 5%, and for large distances ($\rho > 8 \text{ mm}$) the differences are smaller than 1% when the noise in the Monte Carlo simulations is accounted for. In general, the differences are even smaller for turbid media having larger thicknesses, because the diffusion approximation is better fulfilled.

Finally, Fig. 7 shows the transmittance from a four-layered turbid medium having a finite fourth layer. The solution of the diffusion equation (solid line) calculated with Eqs. (26), (24), and (15)–(18) was compared to Monte Carlo simulations (circles). The total thickness of the four layers was 24 mm.

Figure 7 shows good agreement between the two calculations for all distances because in transmission, the diffusion approximation is valid also for small ρ values due to the large value of the product $\mu_s' L_4$, i.e., the transmitted photons have experienced a high number of scattering interactions in the turbid medium. The relative differences between the Monte Carlo simulation and the solutions from the diffusion equation are shown in Fig. 8. The differences are largely caused by the statistics of the Monte Carlo simulations. The systematic differences due to the diffusion approximations are smaller than about 1% for all distances.
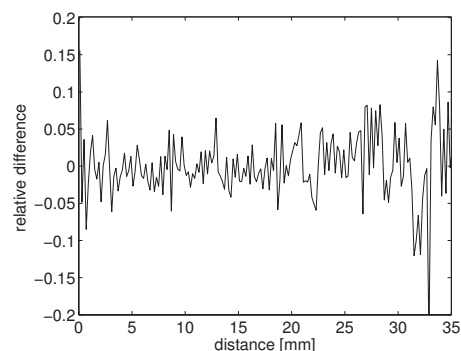

Fig. 8 Relative difference [(Monte Carlo−diffusion)/Monte Carlo] of the curves shown in Fig. 7.

4 Discussion

The solutions of the *N*-layered diffusion equation were calculated in the steady-state domain for turbid media having a finite and an infinitely thick *N*'th layer. Analytical solutions were derived for the fluence rate in the Fourier space. The decisive point for obtaining precise values in real space is the accurate evaluation of the 2-D inverse Fourier transform. To this end, we first derived approximations of the analytical solutions in the Fourier space for large *s* values (see Sec. 5.2). Second, we investigated four different methods for calculation of the inverse Fourier transform. Subsequently, we could estimate the errors of the obtained values for the reflectance and transmittance from the *N*-layered turbid media by comparing the results of the four methods. We found relative differences that were typically smaller than 10^{-7}. These values are a compromise between accuracy and speed of the solutions. Although we emphasized the accuracy in the calculations, we could achieve short calculation times in the range of 10 ms even for a large number of reflectance or transmittance values at different distances from the source.

We compared the solutions of the *N*-layered diffusion equation having an infinite and finite thick *N*'th layer with results from Monte Carlo simulations. The relative differences between both methods were in the same range as those found for homogeneous turbid media having a semi-infinite or slab geometry.[25]

Note that the derived solutions can be easily altered to obtain solutions of the heat conduction equation in an *N*-layered material. Also, different boundary conditions, for example, the partial boundary condition, can be implemented with our method.[22]

In future work, the derived solutions will be used to study the inverse problem. For example, the determination of the optical properties of the brain using a layered model for the head will be investigated. We study whether *a priori* information of, for example, the optical properties of some of the involved tissue layers, is required to derive accurately the optical properties of the brain.

Appendix A. Fluence Rate in Fourier Space

In this subsection we present the analytical solutions of the fluence rate in the Fourier space for turbid media having two,

three, and four layers ($N=2,3,4$). For turbid media having a finite thick *N*'th layer, the fluence rate in the first and *N*'th layer is given, whereas only the fluence rate in the first layer is shown for the case of an infinite thick *N*'th layer.

First, for the fluence rate in the first layer (above the δ source) of the turbid medium having both a finite and infinite thick bottom layer we obtain

$$\Phi_1(z,s) = \frac{\sinh[\alpha_1(z_0 + z_{b_1})]}{\alpha_1 D_1} \frac{Z(z,s)}{N(z,s)} - \frac{\sinh[\alpha_1(z_0 - z)]}{\alpha_1 D_1}. \tag{27}$$

The quantities $N(z,s)$ and $Z(z,s)$ are for a finite two-layered turbid medium:

$$Z(z,s) = \alpha_1 D_1 \sinh[\alpha_2(l_2 + z_{b_2})]\cosh[\alpha_1(l_1 - z)]$$
$$+ \left(\frac{n_2}{n_1}\right)^2 \alpha_2 D_2 \cosh[\alpha_2(l_2 + z_{b_2})]\sinh[\alpha_1(l_1 - z)], \tag{28}$$

$$N(z,s) = \alpha_1 D_1 \sinh[\alpha_2(l_2 + z_{b_2})]\cosh[\alpha_1(l_1 + z_{b_1})]$$
$$+ \left(\frac{n_2}{n_1}\right)^2 \alpha_2 D_2 \cosh[\alpha_2(l_2 + z_{b_2})]\sinh[\alpha_1(l_1 + z_{b_1})], \tag{29}$$

for an infinite two-layered turbid medium:

$$Z(z,s) = \alpha_1 D_1 \cosh[\alpha_1(l_1 - z)] + \left(\frac{n_2}{n_1}\right)^2 \alpha_2 D_2 \sinh[\alpha_1(l_1 - z)], \tag{30}$$

$$N(z,s) = \alpha_1 D_1 \cosh[\alpha_1(l_1 + z_{b_1})]$$
$$+ \left(\frac{n_2}{n_1}\right)^2 \alpha_2 D_2 \sinh[\alpha_1(l_1 + z_{b_1})], \tag{31}$$

for a finite three-layered turbid medium:

$$Z(z,s) = \alpha_1 D_1 \left\{ \alpha_2 D_2 \sinh[\alpha_3(l_3 + z_{b_2})]\cosh(\alpha_2 l_2) + \left(\frac{n_3}{n_2}\right)^2 \alpha_3 D_3 \cosh[\alpha_3(l_3 + z_{b_2})]\sinh(\alpha_2 l_2) \right\} \cosh[\alpha_1(l_1 - z)]$$
$$+ \left(\frac{n_2}{n_1}\right)^2 \alpha_2 D_2 \left\{ \alpha_2 D_2 \sinh[\alpha_3(l_3 + z_{b_2})]\sinh(\alpha_2 l_2) + \left(\frac{n_3}{n_2}\right)^2 \alpha_3 D_3 \cosh[\alpha_3(l_3 + z_{b_2})]\cosh(\alpha_2 l_2) \right\} \sinh[\alpha_1(l_1 - z)], \tag{32}$$

$$N(z,s) = \alpha_1 D_1 \left\{ \alpha_2 D_2 \sinh[\alpha_3(l_3 + z_{b_2})]\cosh(\alpha_2 l_2) + \left(\frac{n_3}{n_2}\right)^2 \alpha_3 D_3 \cosh[\alpha_3(l_3 + z_{b_2})]\sinh(\alpha_2 l_2) \right\} \cosh[\alpha_1(l_1 + z_{b_1})]$$
$$+ \left(\frac{n_2}{n_1}\right)^2 \alpha_2 D_2 \left\{ \alpha_2 D_2 \sinh[\alpha_3(l_3 + z_{b_2})]\sinh(\alpha_2 l_2) + \left(\frac{n_3}{n_2}\right)^2 \alpha_3 D_3 \cosh[\alpha_3(l_3 + z_{b_2})]\cosh(\alpha_2 l_2) \right\} \sinh[\alpha_1(l_1 + z_{b_1})], \tag{33}$$

for an infinite three-layered turbid medium:

$$Z(z,s) = \alpha_1 D_1 \left[\alpha_2 D_2 \cosh(\alpha_2 l_2) + \left(\frac{n_3}{n_2}\right)^2 \alpha_3 D_3 \sinh(\alpha_2 l_2) \right] \cosh[\alpha_1(l_1 - z)] + \left(\frac{n_2}{n_1}\right)^2 \alpha_2 D_2 \left[\alpha_2 D_2 \sinh(\alpha_2 l_2) \right.$$
$$\left. + \left(\frac{n_3}{n_2}\right)^2 \alpha_3 D_3 \cosh(\alpha_2 l_2) \right] \sinh[\alpha_1(l_1 - z)], \tag{34}$$

for a finite four-layered turbid medium:

$$N(z,s) = \alpha_1 D_1 \left[\alpha_2 D_2 \cosh(\alpha_2 l_2) + \left(\frac{n_3}{n_2}\right)^2 \alpha_3 D_3 \sinh(\alpha_2 l_2) \right] \cosh[\alpha_1(l_1 + z_{b_1})] + \left(\frac{n_2}{n_1}\right)^2 \alpha_2 D_2 \left[\alpha_2 D_2 \sinh(\alpha_2 l_2) \right.$$
$$\left. + \left(\frac{n_3}{n_2}\right)^2 \alpha_3 D_3 \cosh(\alpha_2 l_2) \right] \sinh[\alpha_1(l_1 + z_{b_1})], \tag{35}$$

for a finite four-layered turbid medium:

$$\mathcal{Z}(z,s) = \alpha_1 D_1 \left(\alpha_2 D_2 \left\{ \alpha_3 D_3 \sinh[\alpha_4(l_4 + z_{b_2})]\cosh(\alpha_3 l_3) + \left(\frac{n_4}{n_3}\right)^2 \alpha_4 D_4 \cosh[\alpha_4(l_4 + z_{b_2})]\sinh(\alpha_3 l_3) \right\} \cosh(\alpha_2 l_2) \right.$$
$$+ \left(\frac{n_3}{n_2}\right)^2 \alpha_3 D_3 \left\{ \alpha_3 D_3 \sinh[\alpha_4(l_4 + z_{b_2})]\sinh(\alpha_3 l_3) + \left(\frac{n_4}{n_3}\right)^2 \alpha_4 D_4 \cosh[\alpha_4(l_4 + z_{b_2})]\cosh(\alpha_3 l_3) \right\} \sinh(\alpha_2 l_2) \right) \cosh[\alpha_1(l_1 - z)]$$
$$+ \left(\frac{n_2}{n_1}\right)^2 \alpha_2 D_2 \left(\alpha_2 D_2 \left\{ \alpha_3 D_3 \sinh[\alpha_4(l_4 + z_{b_2})]\cosh(\alpha_3 l_3) + \left(\frac{n_4}{n_3}\right)^2 \alpha_4 D_4 \cosh[\alpha_4(l_4 + z_{b_2})]\sinh(\alpha_3 l_3) \right\} \sinh(\alpha_2 l_2) \right.$$
$$+ \left(\frac{n_3}{n_2}\right)^2 \alpha_3 D_3 \left\{ \alpha_3 D_3 \sinh[\alpha_4(l_4 + z_{b_2})]\sinh(\alpha_3 l_3) + \left(\frac{n_4}{n_3}\right)^2 \alpha_4 D_4 \cosh[\alpha_4(l_4 + z_{b_2})]\cosh(\alpha_3 l_3) \right\} \cosh(\alpha_2 l_2) \right) \sinh[\alpha_1(l_1 - z)], \tag{36}$$

$$\mathcal{N}(z,s) = \alpha_1 D_1 \left(\alpha_2 D_2 \left\{ \alpha_3 D_3 \sinh[\alpha_4(l_4 + z_{b_2})]\cosh(\alpha_3 l_3) + \left(\frac{n_4}{n_3}\right)^2 \alpha_4 D_4 \cosh[\alpha_4(l_4 + z_{b_2})]\sinh(\alpha_3 l_3) \right\} \cosh(\alpha_2 l_2) \right.$$
$$+ \left(\frac{n_3}{n_2}\right)^2 \alpha_3 D_3 \left\{ \alpha_3 D_3 \sinh[\alpha_4(l_4 + z_{b_2})]\sinh(\alpha_3 l_3) + \left(\frac{n_4}{n_3}\right)^2 \alpha_4 D_4 \cosh[\alpha_4(l_4 + z_{b_2})]\cosh(\alpha_3 l_3) \right\} \sinh(\alpha_2 l_2) \right) \cosh[\alpha_1(l_1$$
$$+ z_{b_1})] + \left(\frac{n_2}{n_1}\right)^2 \alpha_2 D_2 \left(\alpha_2 D_2 \left\{ \alpha_3 D_3 \sinh[\alpha_4(l_4 + z_{b_2})]\cosh(\alpha_3 l_3) + \left(\frac{n_4}{n_3}\right)^2 \alpha_4 D_4 \cosh[\alpha_4(l_4 + z_{b_2})]\sinh(\alpha_3 l_3) \right\} \sinh(\alpha_2 l_2) \right.$$
$$+ \left(\frac{n_3}{n_2}\right)^2 \alpha_3 D_3 \left\{ \alpha_3 D_3 \sinh[\alpha_4(l_4 + z_{b_2})]\sinh(\alpha_3 l_3) + \left(\frac{n_4}{n_3}\right)^2 \alpha_4 D_4 \cosh[\alpha_4(l_4 + z_{b_2})]\cosh(\alpha_3 l_3) \right\} \cosh(\alpha_2 l_2) \right) \sinh[\alpha_1(l_1$$
$$+ z_{b_1})], \tag{37}$$

for an infinite four-layered turbid medium:

$$\mathcal{Z}(z,s) = \alpha_1 D_1 \left\{ \alpha_2 D_2 \left[\alpha_3 D_3 \cosh(\alpha_3 l_3) + \left(\frac{n_4}{n_3}\right)^2 \alpha_4 D_4 \sinh(\alpha_3 l_3) \right] \cosh(\alpha_2 l_2) + \left(\frac{n_3}{n_2}\right)^2 \alpha_3 D_3 \left[\alpha_3 D_3 \sinh(\alpha_3 l_3) \right. \right.$$
$$\left. + \left(\frac{n_4}{n_3}\right)^2 \alpha_4 D_4 \cosh(\alpha_3 l_3) \right] \sinh(\alpha_2 l_2) \right\} \cosh[\alpha_1(l_1 - z)] + \left(\frac{n_2}{n_1}\right)^2 \alpha_2 D_2 \left\{ \alpha_2 D_2 \left[\alpha_3 D_3 \cosh(\alpha_3 l_3) \right. \right.$$
$$\left. + \left(\frac{n_4}{n_3}\right)^2 \alpha_4 D_4 \sinh(\alpha_3 l_3) \right] \sinh(\alpha_2 l_2) + \left(\frac{n_3}{n_2}\right)^2 \alpha_3 D_3 \left[\alpha_3 D_3 \sinh(\alpha_3 l_3) + \left(\frac{n_4}{n_3}\right)^2 \alpha_4 D_4 \cosh(\alpha_3 l_3) \right] \cosh(\alpha_2 l_2) \right\} \sinh[\alpha_1(l_1$$
$$- z)], \tag{38}$$

$$\mathcal{N}(z,s) = \alpha_1 D_1 \Bigg\{ \alpha_2 D_2 \Bigg[\alpha_3 D_3 \cosh(\alpha_3 l_3) + \left(\frac{n_4}{n_3}\right)^2 \alpha_4 D_4 \sinh(\alpha_3 l_3) \Bigg] \cosh(\alpha_2 l_2) + \left(\frac{n_3}{n_2}\right)^2 \alpha_3 D_3 \Bigg[\alpha_3 D_3 \sinh(\alpha_3 l_3)$$

$$+ \left(\frac{n_4}{n_3}\right)^2 \alpha_4 D_4 \cosh(\alpha_3 l_3) \Bigg] \sinh(\alpha_2 l_2) \Bigg\} \cosh[\alpha_1(l_1 + z_{b_1})] + \left(\frac{n_2}{n_1}\right)^2 \alpha_2 D_2 \Bigg\{ \alpha_2 D_2 \Bigg[\alpha_3 D_3 \cosh(\alpha_3 l_3)$$

$$+ \left(\frac{n_4}{n_3}\right)^2 \alpha_4 D_4 \sinh(\alpha_3 l_3) \Bigg] \sinh(\alpha_2 l_2) + \left(\frac{n_3}{n_2}\right)^2 \alpha_3 D_3 \Bigg[\alpha_3 D_3 \sinh(\alpha_3 l_3) + \left(\frac{n_4}{n_3}\right)^2 \alpha_4 D_4 \cosh(\alpha_3 l_3) \Bigg] \cosh(\alpha_2 l_2) \Bigg\} \sinh[\alpha_1(l_1$$

$$+ z_{b_1})]. \tag{39}$$

Second, for the fluence rate in the *N*'th layer we obtain for the finite two-layered turbid medium:

$$\Phi_2(z,s)$$
$$= \frac{(n_2/n_1)^2 \sinh[\alpha_1(z_0 + z_{b_1})] \sinh[\alpha_2(L_2 + z_{b_2} - z)]}{N(z,s)}, \tag{40}$$

where $N(z,s)$ is given by Eq. (29). For the finite three-layered turbid medium:

$$\Phi_3(z,s)$$
$$= \frac{\alpha_2 D_2 (n_3/n_1)^2 \sinh[\alpha_1(z_0 + z_{b_1})] \sinh[\alpha_3(L_3 + z_{b_2} - z)]}{N(z,s)}, \tag{41}$$

where $N(z,s)$ is given by Eq. (33). For the finite four-layered turbid medium:

$$\Phi_4(z,s)$$
$$= \frac{\alpha_2 D_2 \alpha_3 D_3 (n_4/n_1)^2 \sinh[\alpha_1(z_0 + z_{b_1})] \sinh[\alpha_4(L_4 + z_{b_2} - z)]}{N(z,s)}, \tag{42}$$

where $N(z,s)$ is given by Eq. (37).

Appendix B. Approximate Solutions of the Fluence Rate in Fourier Space

To avoid numerical errors in the computation of the inverse Fourier transform, we derived approximate solutions for the fluence rate of *N*-layered turbid media in the Fourier space. Note that in an earlier paper we derived corresponding results for a two-layered medium.[6] For $2\alpha_1(l_1 + z_{b_1}) \gg 1$ we got

$$\Phi_1(z=0,s) = \frac{1}{2\alpha_1 D_1} (\exp(-\alpha_1 z_0) - \exp[-\alpha_1(z_0 + 2z_{b_1})]$$

$$+ \mathcal{D}_a \{ \exp[\alpha_1(z_0 - 2l_1)] - \exp[\alpha_1(z_0 - 2l_1 - 2z_{b_1})]$$

$$- \exp[\alpha_1(-z_0 - 2l_1 - 2z_{b_1})] - \exp[-\alpha_1(z_0 + 2l_1$$

$$+ 4z_{b_1})]\} + \mathcal{D}_a^2 \{ \exp[\alpha_1(z_0 - 4l_1 - 4z_{b_1})] - \exp[\alpha_1(z_0$$

$$- 2z_{b_1} - 4l_1)] + \exp[\alpha_1(-z_0 - 4l_1 - 4z_{b_1})]$$

$$- \exp[-\alpha_1(z_0 + 4l_1 + 6z_{b_1})]\}), \tag{43}$$

where

$$\mathcal{D}_a = \frac{\alpha_1 \beta_3 D_1 - \alpha_2 \gamma_3 D_2 (n_2^2/n_1^2)}{\alpha_1 \beta_3 D_1 + \alpha_2 \gamma_3 D_2 (n_2^2/n_1^2)},$$

and β_3 and γ_3 are iteratively calculated using Eq. (18). The starting values are obtained from Eq. (17) for a *N*-layered turbid medium having a finite thick *N*'th layer and from Eq. (19) for a turbid medium having an infinitely thick *N*'th layer. This approximation was typically used for *s* values larger than $10/[2(l_1 + z_{b_1})]$.

References

1. A. Ishimaru, *Wave Propagation and Scattering in Random Media*, Academic Press, New York (1978).
2. F. Voit, J. Schäfer, and A. Kienle, "Light scattering by multiple spheres: comparison between Maxwell theory and radiative transfer theory calculations," *Opt. Lett.* **34**(17), 2593–2595 (2009).
3. I. Dayan, S. Havlin, and G. H. Weiss, "Photon migration in a two-layer turbid medium. A diffusion analysis," *J. Mod. Opt.* **39**, 1567–1582 (1992).
4. A. Kienle, M. S. Patterson, N. Dögnitz, R. Bays, G. Wagnières, and H. van den Bergh, "Noninvasive determination of the optical properties of two-layered turbid media," *Appl. Opt.* **37**, 779–791 (1998).
5. A. Kienle, T. Glanzmann, G. Wagnières, and H. van den Bergh, "Investigation of two-layered turbid media with time-resolved reflectance," *Appl. Opt.* **37**, 6852–6862 (1998).
6. A. Kienle and T. Glanzmann, "In vivo determination of the optical properties of muscle using a layered-model," *Phys. Med. Biol.* **44**, 2689–2702 (1999).
7. G. Alexandrakis, T. J. Farrell, and M. S. Patterson, "Accuracy of the diffusion approximation in determining the optical properties of a two-layer turbid medium," *Appl. Opt.* **37**, 7401–7409 (1998).
8. S.-H. Tseng, C. Hayakawa, B. J. Tromberg, J. Spanier, and A. J. Durkin, "Quantitative spectroscopy of superficial turbid media," *Opt. Lett.* **23**, 3165–3167 (2005).
9. G. Alexandrakis, T. J. Farrell, and M. S. Patterson, "Monte Carlo diffusion hybrid model for photon migration in a two-layer turbid medium in the frequency domain," *Appl. Opt.* **39**, 2235–2244 (2000).
10. M. Das, C. Xu, and Q. Zhu, "Analytical solution for light propagation in a two-layer tissue structure with a tilted interface for breast imaging," *Appl. Opt.* **45**, 5027–5036 (2006).
11. J. Li, G. Dietsche, D. Iftime, S. E. Skipetrov, G. Maret, T. Elbert, B. Rockstroh, and T. Gisler, "Noninvasive detection of functional brain activity with near-infrared diffusing-wave spectroscopy," *J. Biomed. Opt.* **10**, 044002 (2005).
12. J.-M. Tualle, J. Prat, E. Tinet, and S. Avrillier, "Real-space Green's function calculation for the solution of the diffusion equation in stratified turbid media," *J. Opt. Soc. Am. A* **17**, 2046–2055 (2000).

13. F. Martelli, A. Sassaroli, S. Del Bianco, Y. Yamada, and G. Zaccanti, "Solution of the time-dependent diffusion equation for layered diffusive media by the eigenfunction method," *Phys. Rev. E* **67**, 056623 (2003).

14. F. Martelli, A. Sassaroli, S. Del Bianco, and G. Zaccanti, "Solution of the time-dependent diffusion equation for a three-layer medium: application to study photon migration through a simplified adult head model," *Phys. Med. Biol.* **52**, 2827–2843 (2007).

15. F. Martelli, S. Del Bianco, and G. Zaccanti, "Perturbation model for light propagation through diffusive layered media," *Phys. Med. Biol.* **50**, 2159–2166 (2005).

16. A. H. Barnett, "A fast numerical method for time-resolved photon diffusion in general stratified turbid media," *J. Comp. Physiol.* **201**, 771–797 (2004).

17. C. Donner and H. W. Jensen, "Rapid simulations of steady-state spatially resolved reflectance and transmittance profiles of multilayered turbid materials," *J. Opt. Soc. Am. A* **23**, 1382–1390 (2006).

18. X. C. Wang and S. M. Wang, "Light transport modell in a *N*-layered mismatched tissue," *Waves Rand. Compl. Media* **16**, 121–135 (2006).

19. J. M. Tualle, H. M. Nghiem, D. Ettori, R. Sablong, E. Tinet, and S. Avrillier, "Asymptotic behavior and inverse problem in layered scattering media," *J. Opt. Soc. Am. A* **21**, 24–34 (2004).

20. A. Liemert and A. Kienle, "Light diffusion in *N*-layered turbid media: frequency and time domain," *J. Biomed. Opt.* **15**(2), 025002 (2010).

21. http://www.uni-ulm.de/ilm/index.php?id=10020200.

22. R. C. Haskell, L. O. Svaasand, T. T. Tsay, T. C. Feng, M. McAdams, and B. J. Tromberg, "Boundary conditions for the diffusion equation in radiative transfer," *J. Opt. Soc. Am. A* **11**, 2727–2741 (1994).

23. W. H. Press, B. P. Flannery, S. A. Teukolsky, and W. T. Vetterling, *Numerical Recipes in Pascal*, Cambridge University, Cambridge, UK (1990).

24. A. E. Siegman, "Quasi fast Hankel transform," *Opt. Lett.* **1**, 13–15 (1977).

25. A. Kienle and M. S. Patterson, "Improved solutions of the steady-state and the time-resolved diffusion equations for reflectance from a semi-infinite turbid medium," *J. Opt. Soc. Am. A* **14**, 246–254 (1997).

26. L. Wang, S. L. Jaques, and L. Zheng, "MCML—Monte Carlo modeling of light transport in multi-layered tissues," *Comp. Meth. Progr. Biomed.* **47**, 131–146 (1995).